Materials Advances

ROYAL SOCIETY OF CHEMISTRY

PAPER

View Article Online
View Journal | View Issue

Cite this: *Mater. Adv.*, 2024, 5, 6234

Synergistic co-adsorptive removal of crystal violet and chromium(VI) from water by pozzolan-charcoal based geopolymer composites

Jacques Madiba Mboka,[a] Hermann Dzoujo Tamaguelon, *[a] Victor Odhiambo Shikuku,[b] Sylvain Tome,[ad] Romain Pokeya,[a] Donald Kamdem Njouond,[e] Fidele Gallo Titini,[a] Aysenur Limon,[c] Christoph Janiak,[c] Marchand Manga Dika,[a] Marie Annie Etoh[a] and David Joh Daniel Dina*[a]

In this study, the geopolymer composites GP_0, $GP_{7.5\text{-}CP}$, and $GP_{10\text{-}CP}$ were synthesized using mixtures of pozzolan (Pz) and waste charcoal powders (CP) as precursors with CP mass contents of 0, 7.5 and 10%, respectively. The geocomposites obtained were characterized by X-ray diffraction (XRD), Fourier transform infrared spectroscopy (FTIR), Brunauer–Emmett–Teller (BET) surface analysis and scanning electron microscopy analysis (SEM). The sequestration performance for crystal violet (CV) and chromium VI (Cr VI) was evaluated in mono- and bi-component systems. The incorporation of 7.5% CP ($GP_{7.5\text{-}CP}$) resulted in a ~19% increase in the specific surface area and densification of the functional groups. Incorporation of CP increased the adsorption capacity due to (1) increased surface areas (2) increased active functional group density and distribution, and (3) shielding effect of CP on acidic sites improving CV adsorption. The adsorption capacities in binary systems were 45 and 59% higher than in single solute systems for CV and Cr(VI), respectively. The $R_q > 1$ and $1/n > 1$ implied synergistic and cooperative adsorption, denoting adsorption of Cr(VI) creates new binding sites for CV adsorption. Ultrahigh adsorption density of 2803 and 3659 mg g^{-1} in single solute systems was achieved for CV and Cr(VI), respectively. The adsorption mechanism is multi-mechanistic involving the reduction of $HCrO_4^-$ to Cr^{3+} by the donor groups of geocomposites, ion exchange, electrostatic and hydrogen bonding interactions. Modification of geopolymers with coal ash stupendously ameliorates their adsorption capacity for simultaneous adsorption of dyes and heavy metals in water.

Received 19th April 2024,
Accepted 27th June 2024

DOI: 10.1039/d4ma00408f

rsc.li/materials-advances

1. Introduction

Geopolymers are a class of eco-materials resulting from a polymerization/polycondensation reaction between amorphous or semi-crystalline aluminosilicate feedstock and alkaline or phosphoric acid solution at ambient temperature or below 100 °C.[1] The aluminosilicate sources preferentially used can be natural (volcanic slag, pozzolana, metakaolin, pumice, and laterite), industrial (fly ash, blast furnace slag, and dolochar)[2,3] or ashes derived from incineration of solid wastes.[4] Surface properties such as specific surface area, cation exchange capacity and functional group identities and distribution make geopolymers excellent low-cost emerging adsorbents for the removal of dyes, toxic metals, personal and pharmaceutical care compounds (PPCCs) and surfactants from wastewater.[5] Dyes and heavy metals constitute a prevalent class of water pollutants. Particularly, due to their high toxicity and low biodegradability, crystal violet (CV) and hexavalent chromium (Cr(VI)) are the pollutants most commonly found in wastewater and are considered the most hazardous to human health and the environment. Their presence in the ecosystem can lead to genotoxicity, respiratory problems, kidney failure and permanent blindness.[6–8] However, recent studies have reported geopolymer adsorption as one of the most effective remediation methods for eliminating these types of pollutants. For example,

[a] *Department of Chemistry, Faculty of Sciences, University of Douala, P.O. Box 24157, Douala, Cameroon. E-mail: hermann.dzoujo@gmail.com; Tel: +237 694622277*
[b] *Department of Physical Sciences, Kaimosi Friends University, P.O. Box 385-50309, Kaimosi, Kenya*
[c] *Institut für Anorganische Chemie und Strukturchemie, Universität Düsseldorf, Universitätsstr. 1D-40225, Düsseldorf, Germany. Tel: +49-211-81-12286*
[d] *Institut für Mineralogie, Leibniz Universität Hannover, Callinstrasse 3, D-30167, Hannover, Germany*
[e] *Department of Process Engineering, Saint Jerome Catholic University Institute, Av. Akwa Koumassi, Douala, Cameroon*

Qiu *et al.*[9] synthesized a fly ash-based geopolymer for Cr(VI) removal and recorded an adsorption capacity of 49.751 mg g^{-1}. Grillo *et al.*[10] reported an adsorption efficiency of 70% of Cr(VI) on pumice-based geopolymers. López *et al.*[11] assessed the CV binding capacity of a bentonite-based geopolymer and reported a sequestration density of 4.36 mg g^{-1}. According to Jacques *et al.*,[12] acidic functional groups negatively impacts the adsorption of CV. Aluminosilicates, such as geopolymers, contain acidic sites which may thus diminish their adsorption potential for CV. This could explain the low adsorption capacity of 11.06 and 4.36 mg g^{-1} for volcanic scoria and bentonite geopolymer materials for CV uptake, respectively.[11,13] Functionalization of geopolymers with the addition of adjuvants to the geopolymeric network makes it possible to improve the adsorptive properties for CV by clouding the acidic sites rendering them inaccessible while providing new active sites for adsorption of both CV and Cr(VI). For example, Sarkar *et al.*[14] synthesized bivalent metal ion-modified geopolymers (Ni-LDSGP and Zn-LDSGP) for fluoride removal. The study revealed that the incorporation of these bivalent ions resulted in their addition to the geopolymer chain and an increase in specific surface area from 30.84 to 58.14 and 53.42 m^2 g^{-1} for Ni-LDSGP and Zn-LDSGP, respectively. The modified geopolymers exhibited superior adsorption capacity for fluoride than pristine sample. In contrast, incorporation of metakaolin (MK) into volcanic ash based geopolymers ameliorated the surface areas with no significant change in adsorption capacity for methylene blue dye. However, the rapidity of the adsorption process increased with increase in MK fraction.[15] Tome *et al.*[16] showed during the synthesis of laterite (LA)-rice husk ash (RHA) geopolymers that the addition of 5% RHA improved the porosity and densification of the functional groups and that the resulting eco-adsorbent had a Malachite Green adsorption capacity 5 times greater than laterite. Zhang *et al.*[17] prepared geopolymer composites based on metakaolin and chitosan (CS) for crystal violet adsorption. They reported that the addition of 1.0% CS resulted in an increase in surface chemical functions and a high porosity of 50.97% of the CS/PG composite, respectively, resulting in a fixation efficiency of ~95% in CV during a continuous treatment of 14 h. He *et al.*[18] synthesized Lithium hydroxide modified geopolymer (Li-ABW) composite for effective Cr(VI) removal from water. They showed that the integration of Li into the geopolymeric network resulted in an increase in specific surface area (~55.75%) and total pore volume (~91.29%) inducing a sequestration removal efficiency of 85.45% generated by electrostatic interactions. The aforementioned geopolymer pretreatment methods have their inherent limitations. The incorporation of monovalent or divalent metals can lead to secondary water pollution in the event of leaching from the geopolymer structure, and the functionalization of the geopolymer can introduce site-specific interactions that can induce specificity in adsorbate binding. Furthermore, most of adsorption studies involving geopolymers entailed adsorption in single-solute systems, and only a few have investigated the co-adsorption behaviour in binary systems. For example, Fang *et al.*[19] prepared geopolymer microspheres based on three solid wastes, coal gangue, fly ash and blast furnace slag, for the mixed adsorption of methylene blue and Cr(VI). In the bi-component system, Cr(VI) was preferentially adsorbed implying antagonistic effects. Yu *et al.*[20] reported the simultaneous removal of Cu^{2+} and Cr(VI) on metakaolin-based geopolymer modified with cetyltrimethylammonium bromide (CTAB). The study showed that pretreatment with CTAB produced a geopolymer composite that could sorb anions without loss of the ability to adsorb cations. In the studies, however, the adsorption rates in binary systems were not examined. Besides equilibrium adsorption capacity, adsorption rates provide an important criterion in selection of adsorbents, especially modified geopolymers.[15] The effect of co-existence of anionic and cationic adsorbates on reaction rates is not well understood. Furthermore, the rarity of industrial waste precursors in many developing countries, particularly in remote areas, limits their exploration whereas the use of CTAB makes synthesis operations more costly than with carbonaceous additives such as carbonized sugarcane bagasse and tyre ash.[21,22] Pozzolan is a plentiful aluminosilicate suitable for geopolymer development.[21] Additionally, geopolymers are known to be better adsorbents than their precursors.[4,13,15,16,23] While the use of coal powders (CPs) as adjuvants in the synthesis of geopolymers is hypothesized to reduce accessibility of CV to the acidic sites, the resultant antagonistic or protagonist effect in the binary elimination of anionic Cr(VI) is also unknown. Furthermore, while adsorption capacities at equilibrium of adsorbents in binary systems have been evaluated, adsorption kinetics/rates in binary systems are seldom evaluated. To date, there is no work reported on the co-elimination of cationic crystal violet and anionic chromium(VI) in binary systems by geopolymer composites. Evaluating the adsorption capacity and rate and potential limitations of these new materials would improve our understanding of their chemistry and effectiveness in multicomponent systems expected in real wastewater. The solidification of coal powder in geopolymers as new composite adsorbents with ultrahigh adsorption capacities for simultaneous sequestration of heavy metal and dye in water presents the novelty of the present work. The present study evaluated and examined the mechanisms associated with the simultaneous sequestration of the toxic cationic CV dye and a hypertoxic heavy metal Cr(VI) in artificial waters under various experimental conditions by pozzolan- and charcoal powder-based geopolymers.

2. Materials and methods

2.1. Chemical reagents

Crystal violet ($C_{25}H_{30}N_3Cl$, 99% purity), potassium dichromate ($K_2Cr_2O_7$, 99.9% purity), methylene blue (99.9% purity), sodium thiosulphate penta hydrate (99. 9% purity), sublimed Iodine (99% purity), sodium silicate (96% purity), sodium chloride (99. 5%), sodium hydroxide (98% purity) and hydrochloric acid (37% purity) were obtained from Sigma-Aldrich. All chemicals were used as is, without further purification.

2.2 Synthesis of geomaterials

The pozzolan (Pz) and charcoal waste (CP) used as aluminosilicate source and an additive, for the synthesis of the geopolymer composites were obtained from a quarry located in the commune of Quanté (latitude 4°; 40′; 39.37″North and longitude 9°; 40′; 56. 34″East) and from an industrial site for the production of commercial domestic charcoal in the Littoral-Cameroon region, respectively. The raw materials were ground and sieved to particle sizes below 100 μm, the resulting powders were washed, and oven dried at 105 °C for 72 hours. The alkaline solution was prepared by first mixing the sodium hydroxide solution (12 M) with a commercial sodium silicate solution (28.7 wt% SiO_2, 8.9 wt% Na_2O and 62.4 wt% H_2O; density 1.37 g mL^{-1}) in a volume ratio of 2.4. The geopolymer composites were synthesized by mixing pozzolan powders initially substituted by varying proportions of 0, 7.5 and 10 wt% charcoal powder with 25.8 g alkaline activator solution. The different paste formulations resulting from homogenization after 10 minutes were moulded in cylindrical PVC tubes (10 × 20 mm), left to rest for 30 minutes and dried in an oven at 60 °C to promote the polymerization/polycondensation process for 4 days.[16] The geomaterial samples labelled GP_0 (pristine), $GP_{7.5\text{-}CP}$ and $GP_{10\text{-}CP}$, corresponding to the different proportions of charcoal, were ground, sieved and washed for 2 hours with demineralized water to remove excess alkali. The samples were then dried for 6 hours in an oven at 105 °C then stored in plastic containers for characterization and adsorption tests.

2.3 Material characterization

The mineralogical composition and crystallinity of the precursors and geomaterials was determined using the Bruker D8 Discovery X-ray diffraction apparatus in the 2θ range from 6° to 80° with a step size of 0.02° for a scan rate of 1 s per step and CuKα radiation at 27.5 kV and 25 mA. The functional groups present in the samples were obtained using Fourier transform infrared (FTIR) spectroscopy. The IR spectra were recorded between 4000 and 400 cm^{-1} with a resolution of 2 cm^{-1} and 32 scans on an infrared spectrometer (Perkin 156 Elmer, Shelton, CT, USA) using the KBr method. Microporosity and mesoporosity of samples from iodine and methylene blue index tests following the protocol described by Dzoujo *et al.*[21] The isotherms resulting from the adsorption–desorption of N_2 at 77 K using a Quantachrome Autosorb AS6AG Station 3 instrument (Quantachrome, Odelzhausen, Germany) were used to calculate the values of the specific surface areas based on the Brunauer–Emmett–Teller (BET) analysis method. The morphology and internal microstructure were visualized by scanning electron microscopy (SEM, Hitachi Ltd, Japan). The PH at which the surface charge of the geomaterials is zero (pH_{PZC}) was determined using the protocol described by Dzoujo *et al.*[24] Here, various 20 mL solutions of NaCl (0.1 M) were initially adjusted to pH (pH_i) values between 2 and 10. A mass of 0.1 g of geoadsorbents was then brought into contact with the various initial NaCl solutions and the whole was left at room temperature for 8 hours. After filtration, the final pH (pH_f) of each solution was carefully measured using a HANNA pH meter. The pH_{PZC} was obtained from the *x*-axis intercept of the curve of ΔpH *versus* pH_i.

2.4 Batch adsorption study

Single and binary adsorption tests of crystal violet (CV) and hexavalent chromium (Cr(VI)) by the geoadsorbents were performed in duplicate in a batch reactor at 25 °C. The effect of the contact time in single solute or bi-component system on adsorption was carried out by contacting 0.1 g of each adsorbent with 40 mL of 120 mg L^{-1} solutions of CV and/or Cr(VI) for time intervals of 10, 20, 30, 60, 90 and 120 minutes. The residual adsorbate concentrations were determined using a UV-visible spectrophotometer at 595 and 540 nm for CV and Cr(VI), respectively. The effect of the initial concentration of the pollutants in single and binary adsorption was also examined by immersing 0.1 g of each adsorbent with 40 mL of CV and/or Cr(VI) solution of different concentrations (10, 30, 60, 90 and 120 mg L^{-1}). The suspensions were kept under stirring until equilibration and then the residual content of each adsorbate was determined. The influence of pH was examined by varying the pH of the CV or/and Cr(VI) solution from 2 to 10 using 0.1 N solutions of HCl and NaOH depending on the desired pH. The variance of the mean residual concentrations was analyzed by one-way ANOVA using SAS software at a confidence level of 95%. The amount adsorbed at any time t (q_t), the equilibrium adsorbed amounts (q_e) and percent removal (%R) were obtained from eqn (1)–(3) respectively.

$$q_t = \frac{(C_i - C_t)V}{m} \quad (1)$$

$$q_e = \frac{(C_i - C_e)V}{m} \quad (2)$$

$$\%R = \frac{(C_i - C_e)}{C_i} \times 100 \quad (3)$$

where C_i (mg L^{-1}), C_t (mg L^{-1}) and C_e (mg L^{-1}) are respectively the initial, time t and equilibrium concentrations of CV or Cr(VI). V (L) and m (g) represent the volume of the CV or Cr(VI) solution and the mass of the geomaterials, respectively.

3. Results and discussion

3.1 Mineralogical analysis

Fig. 1 shows the diffractograms of the CP and Pz precursors and the GP_0 and $GP_{7.5\text{-}CP}$ geomaterials. The CP coal powders consist mainly of amorphous phases (98.65%) and a few traces of quartz (COD_901-3321). Pozzolan (Pz) consists of minerals such as albite (COD_9009663), andesine (COD_900-1031), augite (COD_900-9665), diopsides (COD_900-5280) and hematite (COD_901-5965) and 52.97% amorphous phases. These minerals, originally present in the pozzolan, are still observed after alkalinisation, indicating the low level of their dissolution in the activating solution during the geopolymerisation process. The activation and incorporation of CP led to an increase in the proportion of amorphous phases from 52.97% to 58.44% and

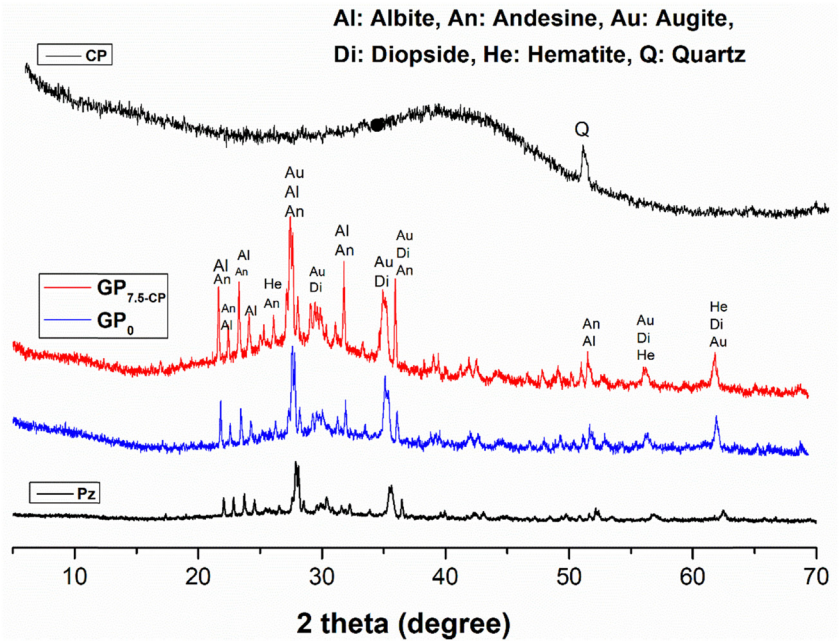

Fig. 1 PXRD patterns of raw material (CP and Pz) and geomaterial (GP_0 and $GP_{7.5\text{-}CP}$).

58.44% to 72.47% for GP_0 and $GP_{7.5\text{-}CP}$, respectively. These changes suggest a restructuring of the geopolymer network with concomitant modification of the textural properties.

3.2 Functions groups analysis

Fig. 2 highlights the FTIR spectrum of CP charcoal powders, pozzolan and GP_0, $GP_{7.5\text{-}CP}$ and $GP_{10\text{-}CP}$ geopolymer composites. In the CP spectrum, the vibrational bands observed between 3896–3743 cm^{-1} and around 3436 cm^{-1} are attributable to the ═C–H bond elongation of vinyl and the O–H bond elongation of alcohols and carboxylic acids, respectively.[25,26] The bands located near 2921 cm^{-1} and centered at 1739 and 1645 cm^{-1} are attributed to C–H bond stretching in aliphatic hydrocarbons and carbonyl stretching, respectively.[27] The peaks located between 1122 and 1037 cm^{-1} are attributable to the C–O stretching vibrations of the carboxylic groups and these derivatives.[28] Those observed at 871, 799, 743, 588 and 422 cm^{-1} reflect the presence of aromatic units within CP structure. In addition, the incorporation of CP during the preparation of $GP_{7.5\text{-}CP}$ and $GP_{10\text{-}CP}$ geopolymer composites is responsible for the appearance of new bending vibration bands of ═C–H of vinyl groups and O–C–O of carbonates observed at 3745–3776 cm^{-1} and 1424–1440 cm^{-1}, respectively, compared with the pristine GP_0 geopolymer. However, a structural reorganization during geopolymerization and the integration of CP into the network is also observed due to the shift in the vibrational bands of the aluminosilicates from 1025 to 1005 cm^{-1}.[29,30] These notable changes corroborate the results of the XRD analysis and could significantly improve the affinity for Cr(VI) and textural properties of the resulting composites.

3.3 Textural analysis

Table 1 shows the results relating to the specific surface areas and iodine and methylene blue indices used to assess the

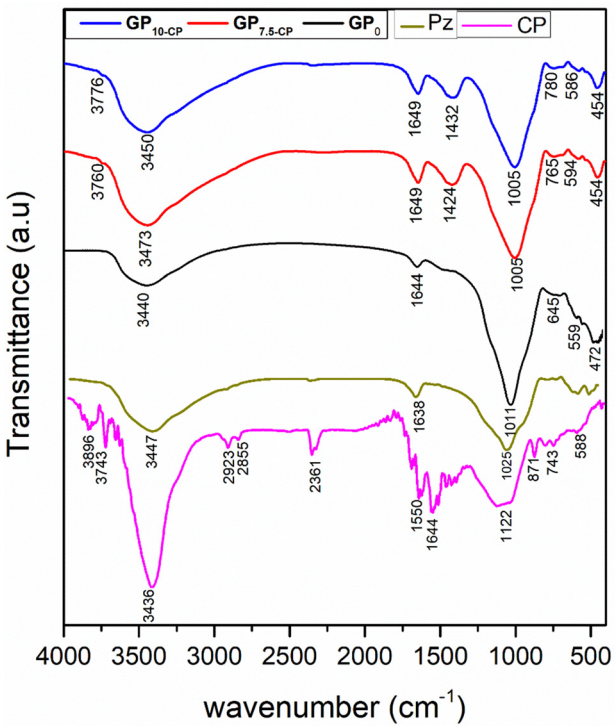

Fig. 2 FTIR spectrum of coal powders, pozzolan and geopolymer composites.

porosity of geomaterials. Geopolymerization and the incorporation of 7.5% CP favored the formation of a microporous rather than mesoporous geopolymeric structure. Above 7.5% CP, the excess dose reduces this microporosity. Furthermore, the increase and reduction in specific surface area of ~19% and ~22% respectively for $GP_{7.5\text{-}CP}$ and $GP_{10\text{-}CP}$ compared with GP_0

Table 1 Specific surface area, microporosity and mesoporosity indices values

Adsorbents	Iodine index (mg g^{-1})	Methylene blue index (mg g^{-1})	Specific surface area (m^2 g^{-1})
CP	659.88	14.28	133.86
GP_0	794.50	15.63	13.35
$GP_{7.5\text{-}CP}$	805.47	15.93	15.89
$GP_{10\text{-}CP}$	748.71	15.65	10.40

corroborate the microporosity of these geocomposites. Although the specific surface areas of these geopolymer composites are lower than those of the functionalized polymers (63.17 m^2 g^{-1} for PAN/ZnO-PNC and 65.40 m^2 g^{-1} for iron oxide-PANI-PNC respectively) reported in the work by Deb *et al.*,[31] Deb *et al.*,[32] the density of the functional group provided by the CPs will be able to compensate for this deficit during the adsorption process.

Fig. 3 shows the micrographs of CP (a) charcoal powders and GP_0 (b), $GP_{7.5\text{-}CP}$ (c) and $GP_{10\text{-}CP}$ (d) geoadsorbents. It can be seen that CP has a heterogeneous and very porous microstructure (Fig. 3a), unlike the GP_0 microstructure (Fig. 3b), which is dense and heterogeneous as a result of the polymerization/polycondensation process and the low dissolution of aluminosilicate phases in the alkaline solution.[33] The microstructures of $GP_{7.5\text{-}CP}$ and $GP_{10\text{-}CP}$ (Fig. 3c and d) show that the addition of CP to the geopolymeric network leads to an increase in porosity, which evolves with the specific surface area. These structural changes are consistent with the results of the XRD and FTIR analyses. However, the increase in specific surface area and functional groups is one of the advantages that could favor the simultaneous sequestration of CV and Cr(VI).

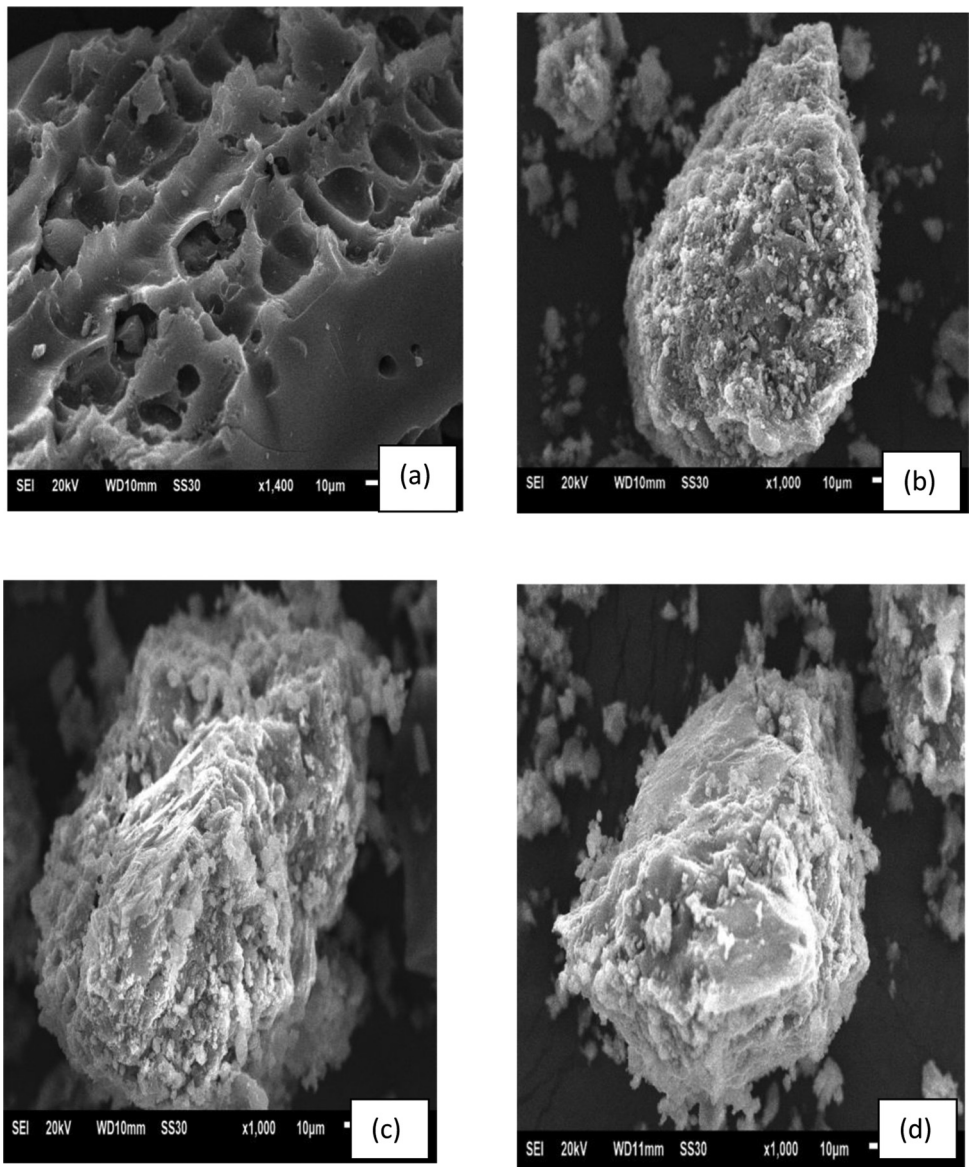

Fig. 3 Micrographs of CP (a) and geoadsorbents GP_0 (b), $GP_{7.5\text{-}CP}$ (c) and $GP_{10\text{-}CP}$ (d).

3.4. Effect of pH in single and binary systems

Fig. 4 and 5 show the pH_{PZC} of the different geopolymers and the evolution of adsorption capacities linked to pH variation in single and bi-component adsorption of CV and Cr(VI). The pH at the zero charge point of the geoadsorbents is between 8 and 9 due to the activating agent used during synthesis. The slight decrease in the pH_{PZC} values of the geopolymer composites compared with the pristine geopolymer denote changes in distribution of the acidic Lewis and Brønsted sites with the incorporation of CP.[12] Furthermore, at pH < pH_{PZC}, single solute retention of CV is unfavorable (Fig. 5a) due to repulsive interactions between the positive surface charges of the geoadsorbents and CV. This is also attributed to increase in Lewis acidic sites at pH < pH_{PZC} which is detrimental for CV uptake.[12] At very pH (>8), the excess Na^+ ions compete for the same binding sites with CV, reducing the number of available adsorption sites with concomitant repulsion between the adsorbed CV molecules and those in bulk solution. In contrast, monocomponent adsorption of Cr(VI) is favored since at 2 < pH < 6 (Fig. 5b), since hexavalent chromium exists as an anionic hydrogen chromate ($HCrO_4^-$) favoring attractive interactions with the positive surface charge of the geomaterials with maximum adsorption at pH 6. However, at low pH, it is conceivable that the high concentration of H^+ affect the second hydration shells surrounding the Cr(VI) ions hindering effective adsorbent–adsorbate interactions. Additionally, competition between the chloride ions from HCl and the anionic Cr(VI) ions also account for the decreased adsorption at low pH. At pH > pH_{PZC}, the geomaterials carry a negative surface charge that favors the retention of CV and hinders the fixation of Cr(VI), which is in the form of CrO_4^{2-} at pH > 6. A similar phenomenon was observed during the bicomponent sequestration of CV and Cr(VI) on the surface of the geoadsorbents (Fig. 5c), with the exception of the strong competition between the adsorbates, which favored an increase in the quantities adsorbed and was later confirmed by the adsorption isotherms. The studies show that the adsorption of Cr(VI) provides new energetically favorable sites for adsorption of additional CV molecules. These results do not corroborate the work of Fang *et al.*[19] which reported that the adsorption capacity of MGP geopolymer microspheres for MB and Cr(VI) in the binary system decreased when the pH increased compared to a single solute system.

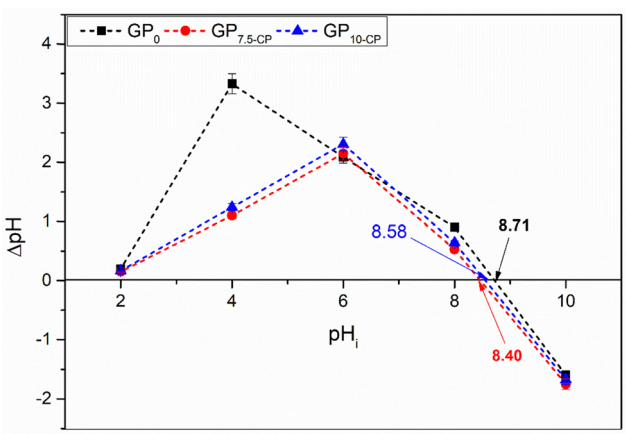

Fig. 4 Point of zero charge of geomaterials.

3.5. Effect of contact time in single and binary systems

Fig. 6 shows the evolution of the quantities of CV and Cr(VI) adsorbed over time. In a monocomponent system (Fig. 6a and b), rapid fixation of CV or Cr(VI) is observed during the first 10 minutes, followed by moderate and slow adsorption beyond the 10th minute. These observations respectively reflect an external and internal mass transfer of CV or Cr(VI) from the solution to the plentiful vacant active sites and mark the progressive saturation of these sites and migration of the adsorbates to the inner pores. However, the slight desorption observed within the GP_0 and $GP_{7.5\text{-}CP}$ geoadsorbents (Fig. 6b) around 10–30 minutes is due to the electrostatic repulsion between the Cr(VI) ions in solution and those in solid phase before equilibration. On the other hand, in the binary system (Fig. 6c), CV binds preferentially before Cr(VI) within the geoadsorbents due to the more hydrophobic nature of CV compared with Cr(VI). However, the desorption phenomena observed at the surface of the geoadsorbents are due to the competitive effect between CV and Cr(VI) for the same active site. However, this phenomenon is more pronounced on the surface of the GP_0 geopolymer due to its fewer sites than those of the $GP_{7.5\text{-}CP}$ and $GP_{10\text{-}CP}$ geocomposites.

3.6. Effect of initial concentration of adsorbates in single and binary systems

Fig. 7 shows the influence of the initial concentration of the single and binary systems on the quantities of adsorbate adsorbed and the removal rate. It was found that the concentration gradient accelerated the process of diffusion and fixation of both CV and Cr(VI) on the geoadsorbents, and consequently an increase in the quantities adsorbed in single and binary systems. Furthermore, at the maximum concentration of 120 mg L^{-1}, an improvement in CV and Cr(VI) adsorption performance was observed in the binary regime (2.15 and 17.97% for GP_0, 3.25 and 34.29% for $GP_{7.5\text{-}CP}$, 4.24 and 7.95% for $GP_{10\text{-}CP}$ respectively) compared with the single solute system. In the mixed system, an increase in the rate of elimination of CV (from 73.60 to 95.76% for GP_0, from 93.86 to 96.06% for $GP_{7.5\text{-}CP}$ and from 91.26 to 95.76% for $GP_{10\text{-}CP}$ respectively) and Cr(VI) (from 5.88 to 67.83% for GP_0, from 6.86 to 70.17% for $GP_{7.5\text{-}CP}$ and from 5.88 to 70.17% for $GP_{10\text{-}CP}$ respectively) was also observed with the initial concentration of adsorbates. The increased adsorption in bi-component system is attributed to the clouding effect of CP to the acidic sites thus improving the uptake of CV with concomitant generation of new adsorption sites for the adsorption of Cr(VI). The adsorbed Cr(VI) ions are also thought to create new surfaces for adsorption of CV.

3.7 Single and binary adsorption kinetics

To elucidate the phenomena governing mono and bi-component adsorption kinetics, non-linear kinetic models of pseudo-first-order,[34] pseudo-second-order[35] and intraparticle diffusion[36]

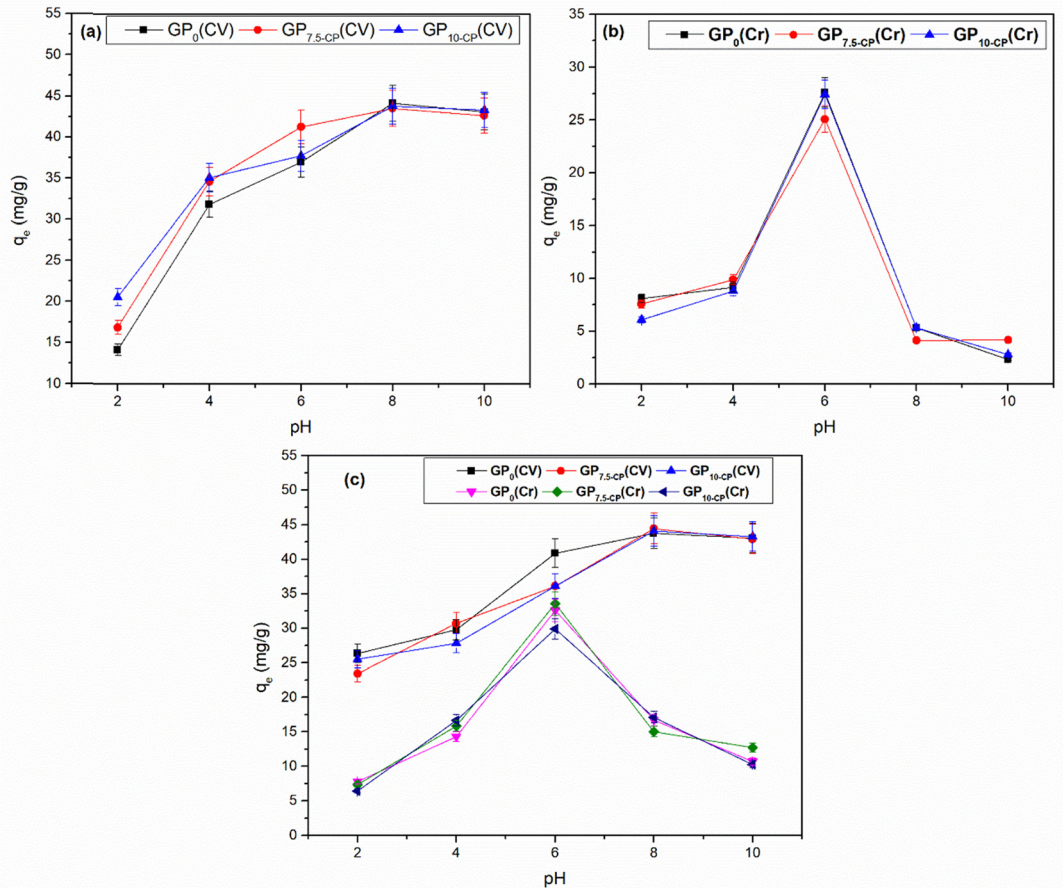

Fig. 5 Influence of pH in single (a), (b) and binary (c) retention of CV and Cr(VI) on geomaterials. Experimental conditions (m_{GP} = 0.1 g, V = 40 mL, T = 25 ± 1 °C, C_i = 120 mg L^{-1} and t = 60 min).

defined by eqn (4), (5) and (7), respectively, were correlated with the experimental contact time data.

$$\text{Pseudo first order (PFO): } q_t = q_e(1 - e^{-k_1 t}) \quad (4)$$

$$\text{Pseudo second order (PSO): } q_t = \frac{k_2 q_e^2 t}{1 + k_2 q_e t} \quad (5)$$

$$t_{1/2} = \frac{1}{K_2 q_e} \quad (6)$$

$$\text{Intraparticle diffusion (ID): } q_t - K_{id} t^{1/2} + C \quad (7)$$

where: q_t and q_e are, respectively, the adsorbed amount (mg g^{-1}) at time t (min) and at equilibrium, respectively. k_1 (min^{-1}) and k_2 (g mg^{-1} min^{-1}) represents the PFO and PSO rate constants, respectively. $t_{1/2}$ is the half adsorption time. K_{id} is the intraparticle diffusion rate constant (mg g^{-1} $min^{-1/2}$), C (mg g^{-1}) is the boundary layer effect index, which provides information about the thickness of the boundary layer.

The coefficients of determination R^2 (Tables 2 and 3), which converge towards unity, show that the PFO, PSO and ID models correlate perfectly with the experimental data for the two systems studied. However, the values of $t_{1/2}$ calculated from eqn (6), which decrease drastically as a function of the CP incorporation rate in single and binary solute adsorption, indicate the increased availability of new functional sites for co-adsorption of CV and Cr(VI). The non-zero values for boundary layer C indicate that diffusion of CV and Cr(VI) into the pores of the geoadsorbents is not the only process governing the rate of adsorption in the two systems studied, which corroborates the results of the work by Deb *et al.*[37] on the sono-assisted adsorption of a binary mixture of dyes (MO and EY) on hematite-PANI-NC. However, the very low K_{id} values and the increase in the Cr(VI) diffusion boundary layer in mixed solution compared with that in monocomponent solution indicate an increase in the mass transfer into the internal pores induced by the presence of CV.

Furthermore, the values of the parameter $1/n > 1$ and Gibb's free energy $\Delta G < 20$ kJ mol^{-1} from the isotherms (Tables 4 and 5) succinctly demonstrated later that physisorption is the rate-determining step governing the fixation of CV and Cr(VI) in binary system.

3.8 Single and binary adsorption isotherms

To understand the observed synergistic effect and mechanisms associated with the retention of CV or Cr(VI) in single or binary regimes, experimental equilibrium data were correlated with Langmuir, Freundlich and Flory Huggins isotherm models.

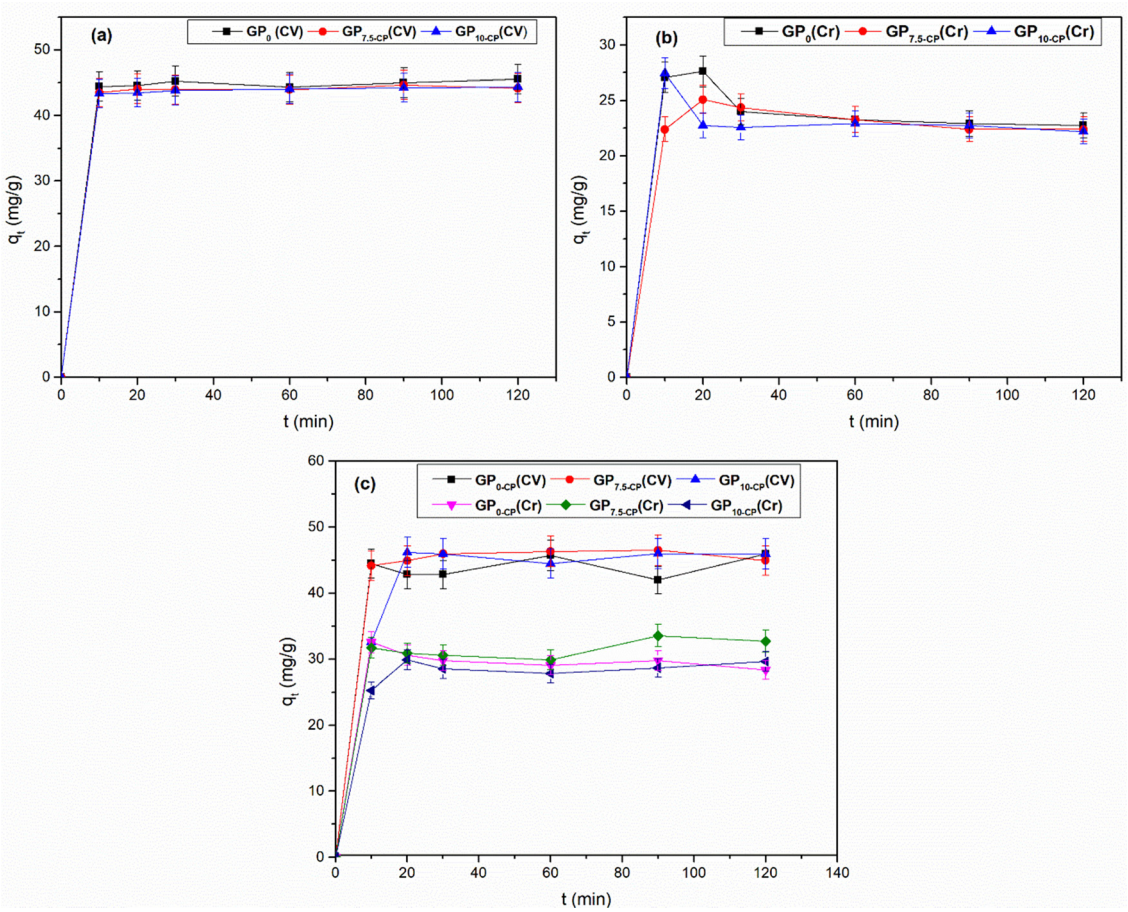

Fig. 6 Effect of contact time on CV and Cr(VI) fixation performance of geomaterials in single (a), (b) and binary (c) systems. Experimental conditions (m_{GP} = 0.1 g, V = 40 mL, T = 25 ± 1 °C and C_i = 120 mg L^{-1}).

3.8.1 Langmuir isotherm. Langmuir's isotherm is an empirical model designed to describe monolayer-binding mechanisms inducing a uniform distribution of adsorbates on homogeneous active sites on the surface of the adsorbent.[38] The Langmuir model equation and the related separation factor are defined by eqn (8) and (9) respectively:

$$q_e = \frac{Q_m K_L C_e}{1 + K_L C_e} \quad (8)$$

$$R_L = \frac{1}{1 + K_L C_0} \quad (9)$$

where q_e and Q_m are respectively the equilibrium adsorbate quantity (mg g^{-1}) and the maximum Langmuir sequestration capacity (mg g^{-1}), C_e is the equilibrium adsorbate content in solution (mg L^{-1}) and K_L is the Langmuir constant (L g^{-1}).

The effect of the simultaneous presence of CV and Cr(VI) on the sequestration efficiency of the bi-component on geomaterials was assessed by calculating the equilibrium adsorption capacity ratio (R_q), defined according to the work of Shikuku *et al.*[39] as follows:

$$R_{q,i} = \frac{q_{b,i}}{q_{s,i}} \quad (10)$$

where $q_{b,i}$ and $q_{s,i}$ are the equilibrium adsorption densities (q_e) of the pollutant i in the bi-component and single solute solutions, respectively. If $R_{q,i} > 1$, the binding of adsorbate i is enhanced by the presence of another adsorbate in a binary system (synergistic adsorption), if $R_{q,i} = 1$, the retention of adsorbate i is unaffected by the presence of the other pollutant in the binary system and if $R_{q,i} < 1$, the presence of the other adsorbate in the binary system exacerbates the sequestration of pollutant i (antagonistic adsorption).

With reference to $R^2 > 0.90$, the Langmuir isotherm is appropriate for describing the retention mechanisms of CV and Cr(VI) on the $GP_{7.5\text{-}CP}$ geocomposite in a single system (Table 4) and on $GP_{10\text{-}CP}$ in a binary system (Table 5). The R_L values indicate that the adsorption of these adsorbates is favorable on the surface of these geopolymer composites, whatever the system. However, the maximum adsorption capacity of CV or Cr(VI) adsorbed predicted in a single system from this model for the $GP_{7.5\text{-}CP}$ geocomposite are respectively ~2 to ~5 times greater than those of the pristine geopolymer. This is due to the threefold positive contributions of higher specific surface area, the new binding sites provided by the incorporation of CP and shielding effect of CP to the acidic sites that negatively impact the adsorption of CV. In addition, a 45% increase in the maximum adsorption density of CV adsorbed on

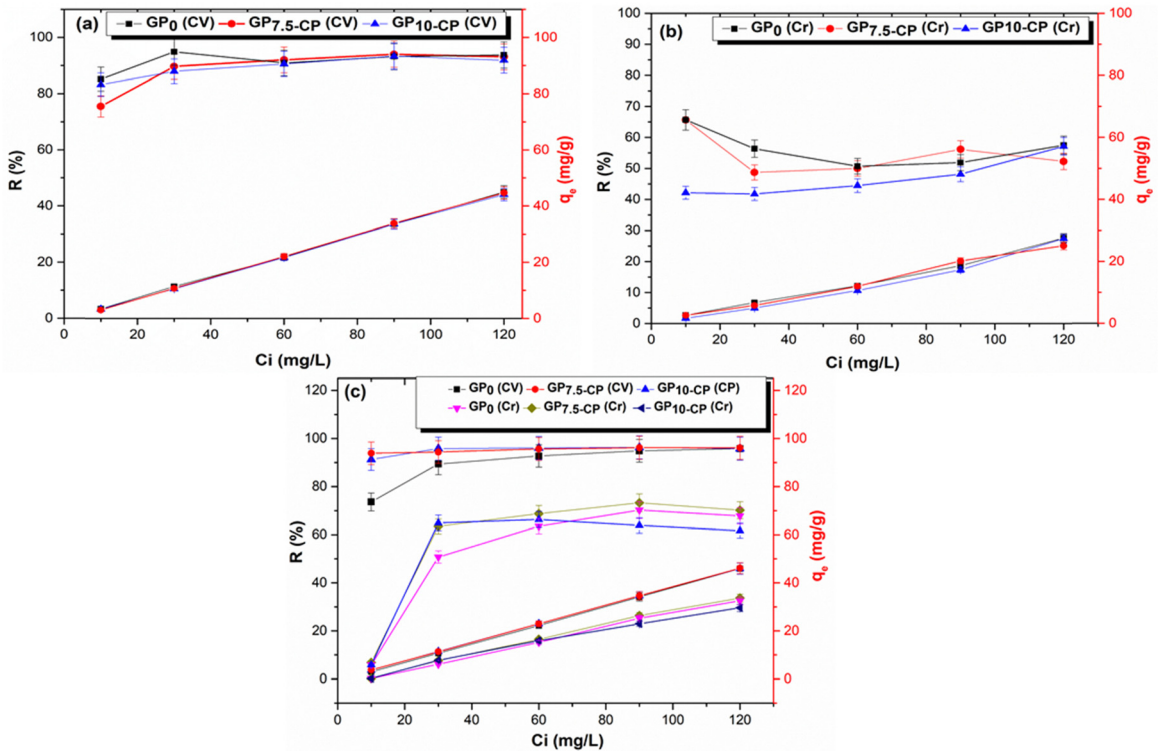

Fig. 7 Effect of initial concentration on single (a), (b) and binary (c) adsorption of CV and Cr(VI) on geomaterials. Experimental conditions (m_{GP} = 0.1 g, V = 40 mL, T = 25 ± 1 °C and t = 60 min).

Table 2 Parameters resulting from kinetic models of CV and Cr(VI) adsorption in a single system

Models	Parameters	GP_0		$GP_{7.5\text{-}CP}$		$GP_{10\text{-}CP}$	
		CV	Cr(VI)	CV	Cr(VI)	CV	Cr(VI)
PFO	k_1 (min^{-1})	2.00	1.60	1.99	0.32	0.47	1.27
	q_e (theor) (mg g^{-1})	44.85	24.60	44.06	23.48	43.83	23.43
	q_e (exp) (mg g^{-1})	45.55	27.61	44.67	25.08	44.33	27.43
	R^2	0.99	0.96	0.99	0.99	0.99	0.96
PSO	k_2 (g mg^{-1} min^{-1})	2.39	8.00	0.14	1.00	0.09	7.99
	q_e (theor) (mg g^{-1})	45.97	24.60	44.37	23.37	44.29	23.46
	q_e (exp) (mg g^{-1})	45.55	27.61	44.67	25.08	44.33	27.43
	$t_{1/2}$ (min)	0.003	0.32	0.003	0.04	0.002	0.34
	R^2	0.99	0.96	0.99	0.99	0.99	0.96
ID	K_{id} (mg g^{-1} $min^{-1/2}$)	0.09	0	0.01	0	0.13	0
	C (mg g^{-1})	44.16	24.60	43.98	23.31	42.99	23.43
	R^2	0.99	0.96	0.99	0.99	0.99	0.96

Table 3 Parameters resulting from kinetic models of CV and Cr(VI) adsorption in a binary system

Models	Parameters	GP_0		$GP_{7.5\text{-}CP}$		$GP_{10\text{-}CP}$	
		CV	Cr(VI)	CV	Cr(VI)	CV	Cr(VI)
PFO	k_1 (min^{-1})	1.60	1.60	0.33	0.94	0.14	0.22
	q_e (exp) (mg g^{-1})	45.97	32.56	46.51	33.54	46.16	29.89
	q_e (theor) (mg g^{-1})	43.95	30.01	45.76	31.56	46.21	28.91
	R^2	0.99	0.99	0.99	0.99	0.99	0.99
PSO	k_2 (g mg^{-1} min^{-1})	2.39	79.25	0.26	0.12	0.01	0.03
	q_e (exp) (mg g^{-1})	45.97	32.56	46.51	33.54	46.16	29.89
	q_e (theor) (mg g^{-1})	43.96	30.02	45.44	31.84	48.68	29.55
	$t_{1/2}$ (min)	0.05	2.64	0.01	0.003	0.0001	0.001
	R^2	0.99	0.99	0.99	0.99	0.97	0.99
ID	K_{id} (mg g^{-1} $min^{-1/2}$)	0.16	0	0.07	0	1.05	0.28
	C (mg g^{-1})	42.87	30.01	44.81	31.56	36.26	26.33
	R^2	0.99	0.99	0.99	0.99	0.94	0.99

$GP_{7.5\text{-}CP}$ and a 59% increase in the quantity of Cr(VI) adsorbed on $GP_{10\text{-}CP}$ was observed in the binary system compared with the single system, revealing that adsorption performance is not solely dependent on specific surface area and surface functional groups. In addition, the values of the equilibrium adsorption capacity ratio R_q for CV and Cr(VI) (Table 6) are greater than unity, indicating an increase (synergism) during co-adsorption in the binary system. This supports the hypothesis that adsorbed Cr(VI) provides new adsorption sites for removal of CV and the steric hindrance from adsorbed molecules shield CV molecules from the acidic sites. This phenomenon implies, mechanisms for attaching CV and Cr(VI) to the surface of the composites are different. The ultrahigh maximum adsorption capacities for CV exceed those reported for CV adsorption by geopolymers indicating the incorporation of CP was beneficial.

3.8.2 Freundlich isotherm. The Freundlich isotherm usually describes the multilayer adsorption of adsorbates on heterogeneous and non-energetically equivalent active sites.[40] The expression of this model is defined by eqn (11).

$$q_e = K_F C_e^{1/n} \quad (11)$$

Table 4 parameters resulting from CV and Cr(VI) adsorption isotherms in a single system

		GP_0		$GP_{7.5\text{-}CP}$		$GP_{10\text{-}CP}$	
Isotherms	Parameters	CV	Cr(VI)	CV	Cr(VI)	CV	Cr(VI)
Langmuir	Q_{max} (mg g^{-1})	1803	784	2803	3659	1632	1164
	K_L (L mg^{-1})	0.01	0.0006	0.01	0.0001	0.01	0.0004
	R_L	0.74	0.93	0.99	0.99	0.97	0.98
	R^2	0.89	0.95	**0.98**	0.97	0.86	0.86
Freundlich	$1/n$	1.19	1.19	0.58	1.01	1.44	1.92
	K_F(L mg^{-1})	3.38	0.23	12.05	0.43	2.59	0.01
	R^2	**0.94**	0.96	0.53	0.97	0.27	0.95
Flory Huggens	K_{FH}	0.79	0.55	0.82	0.53	0.82	0.52
	ΔG (kJ mol^{-1})	−16.54	−15.63	−16.62	−15.54	−16.62	−15.50
	n_{FH}	0	0	0	0	0	0
	R^2	0.92	0.99	0.99	0.99	0.99	0.97

Table 5 parameters resulting from CV and Cr(VI) adsorption isotherms in a binary system

		GP_0		$GP_{7.5\text{-}CP}$		$GP_{10\text{-}CP}$	
Isotherms	Parameters	CV	Cr(VI)	CV	Cr(VI)	CV	Cr(VI)
Langmuir	Q_{max} (mg g^{-1})	6773	1866	4056	1749	2274	1851
	K_L (L mg^{-1})	0.001	0.0004	0.002	0.0005	0.004	0.0003
	R_L	0.90	0.95	0.99	0.98	0.98	0.98
	R^2	0.57	0.84	0.97	0.87	0.97	0.92
Freundlich	$1/n$	3.80	1.49	1.25	1.29	1.03	1.05
	K_F (L mg^{-1})	0.10	0.15	6.85	0.35	9.01	0.56
	R^2	0.98	0.93	0.99	0.91	0.97	0.92
Flory Huggens	K_{FH}	0.95	0.67	0.96	0.70	0.96	0.63
	ΔG (kJ mol^{-1})	−16.98	−16.13	−17.01	−16.25	−17.01	−15.96
	n_{FH}	0	0	0	0	0	0
	R^2	0.99	0.98	0.99	0.98	0.99	0.98

Table 6 Single and binary adsorption of CV and Cr(VI) on geomaterials

	GP_0		$GP_{7.5\text{-}CP}$		$GP_{10\text{-}CP}$	
	CV	Cr(VI)	CV	Cr(VI)	CV	Cr(VI)
$q_{b,i}$	45.97	32.56	46.51	33.54	46.16	29.89
$q_{s,i}$	45.55	27.61	44.67	25.08	44.33	27.43
$R_{q,i}$	1.01	1.18	1.04	1.34	1.04	1.10

where, K_F (L g^{-1}) is the Freundlich constant and n is the Freundlich coefficient.

The values of $R^2 > 0.90$ (Table 5) attest to the adaptability of the Freundlich model in correlating equilibrium data for the mixed adsorption of CV and Cr(VI) for all geoadsorbents. However, values of the Freundlich coefficient $1/n$ greater than unity reflect cooperative sequestration inducing multiple mechanisms relating to the S-type adsorption isotherm describing strong competition between adsorbates in solution for active sites.[41] The cooperative adsorption further supports the postulate that adsorbed Cr(VI) provide new surfaces for adsorption of CV. Furthermore, the higher K_F values for CV than for Cr(VI) indicate the high affinity of geocomposites to bind CV in the CV-Cr(VI) system. This difference is linked to four factors; incorporation of CP provided new functional group density and distribution, increased surface area increased accessibility to the active sites, CP clouded the acidic sites that diminish CV adsorption and adsorbed Cr(VI) provided new surfaces for cooperative adsorption of CV. It is further postulated that the presence of Cr(VI) decreased the equilibrium solubility of CV increasing the distribution of CV between the adsorbent and the bulk solution.

3.8.3 Flory Huggins model. The Flory Huggins isotherm was developed to define the feasibility and spontaneity of adsorbate attachment mechanisms to the adsorbent surface.[42] The mathematical expression of this isotherm is given by eqn (12).

$$\frac{\theta}{c_0} = K_{FH}(1-\theta)^{n_{FH}} \quad \text{with } \theta = 1 - \frac{c_e}{c_0} \tag{12}$$

where K_{FH} (L g^{-1}) is the Flory Huggens equilibrium constant, ΔG (kJ mol^{-1}) is the Gibbs free energy (eqn (13)) calculated from K_{FH} and the density of water φ_W (1000 g L^{-1}).

$$\Delta G = -RT \ln K_{FH}\varphi_W \tag{13}$$

The relatively high coefficients of determination (Tables 4 and 5) show that the Flory Huggens model adjusts the data to equilibrium during the sequestration of CV and Cr(VI) on geoadsorbents in both single and binary systems. Furthermore,

the negative values and $\Delta G < 20$ kJ mol^{-1} indicate respectively that the CV and Cr(VI) fixation process is thermodynamically spontaneous, and that physical-type interactions are predominant at the geomaterial surface favoring PFO kinetics.

Table 7 Comparative data on CV and Cr(VI) sequestration capacities between the geoadsorbents studied and those from previous work

	CV			Cr(VI)			
Adsorbent	Adsorption capacity in single system (mg g^{-1})	Adsorption capacity in binary system (mg g^{-1})	Adsorption type	Adsorption capacity in single system (mg g^{-1})	Adsorption capacity in binary system (mg g^{-1})	Adsorption type	Ref.
Ni/Al@PAB	—	—	—	271.50	NR	Synergistic	43
CTAB modified geopolymers	—	—	—	61.30	95.30	Synergistic	20
LDH/MOF HNC	—	—	—	787	733	NR	44
S-nZVI@ZSM-5	—	—	—	52.16	19.26	Antagonistic	45
FeYBC	—	—	—	24.37	NR	NR	46
Microsphere	—	—	—	26.80	27.12	Antagonistic	19
Surfactant modified alumina	254.30	200.44	Antagonistic	—	—	—	47
Surfactant modified Spirulina sp.	101.87	4.55	Antagonistic	—	—	—	48
NMWNS	123.20	96.01	Antagonistic	—	—	—	49
BDHMP-Vt	956.20	NR	Antagonistic	—	—	—	50
Magnetized polypeptidylated-Hb composites	NR	14.8	Antagonistic	—	—	—	51
CsTC1 composite	37	NR	NR	—	—	—	52
GP_0	1803	6773	Synergistic	784	1866	Synergistic	This study
$GP_{7\text{-}5\text{-}CP}$	2803	4056	Synergistic	3659	1749	Synergistic	This study
$GP_{10\text{-}CP}$	1632	2274	Synergistic	1632	1851	Synergistic	This study

NR: not reported.

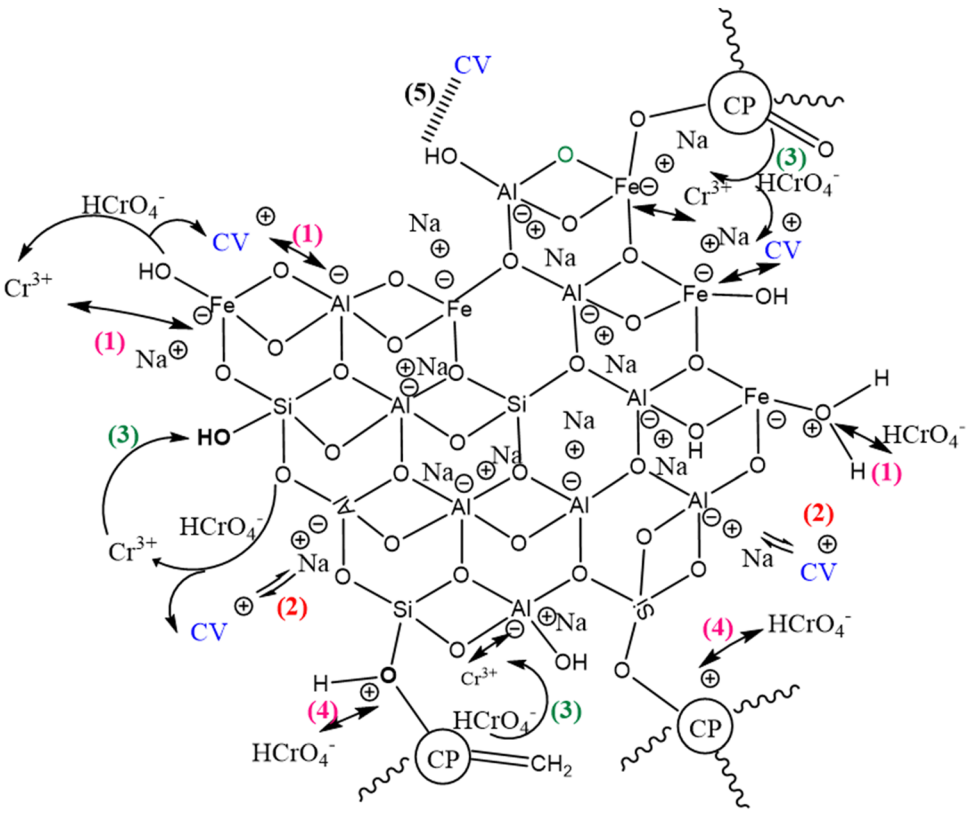

Fig. 8 Probable mechanism for simultaneous fixation of CV and Cr(VI) on the GP-TA eco-composite.

3.9 Adsorption mechanism and comparison with other adsorbents

Table 7 compares the adsorption performance of the geopolymer adsorbents in this study in single and binary systems with other adsorbents in the literature. It was observed that the binding performance of the eco-adsorbents in this study for CV and Cr(VI) was ultrahigh compared with that reported by other adsorbents for both single and binary systems. This difference is linked to the synergistic effect of the adsorbents and the high active functional groups density.

Taking into account the effect of pH and adsorption isotherms, the probable mechanisms (Fig. 8) linked to the ultrahigh performance of GP-CP eco-geocomposite for CV and Cr(VI) in bi-component system include:

– The reduction of $HCrO_4^-$ to Cr^{3+} by the electron-donating groups of the geopolymeric chain, favoring respectively the electrostatic attraction of CV and Cr^{3+} (1) and the exchange of ions (2) on the acid sites of the GP-TA.

– The reduction of $HCrO_4^-$ to Cr^{3+} by the electron-donating groups of CP combined with electrostatic attraction (3).

– Electrostatic attraction of $HCrO_4^-$ to the basic sites of GP-CP (4).

– The formation of hydrogen bonds between CV and the composite surface (5).

These mechanisms are not similar to those reported in the work of Fang *et al.*[19] The authors mentioned that the adsorption of MB in the binary system is controlled mainly by diffusion in the pores, the formation of hydrogen bonds and electrostatic interactions, whereas the fixation of Cr(VI) is governed by diffusion in the pores and redox reactions. The mechanisms controlling the attachment of adsorbates in a mixed system to the surface of the adsorbent depend not only on the composition and textural properties of the geoadsorbent but also on the interactions produced by these adsorbates.

4. Conclusion

This study evaluated single solute and bi-component adsorption of crystal violet (CV) and hexavalent chromium (Cr(VI)) on pozzolan-charcoal powder (CP) waste based geopolymer composites. Physicochemical characterization revealed a 72.47% amorphisation of the geopolymeric structure with the incorporation of 7.5% CP, resulting in a 19% increase in the specific surface area and densification of the functional groups of the resulting $GP_{7.5\text{-}CP}$ composite. The adsorption performance of both CV or Cr(VI) were 45 and 59% higher in binary system than in unary system, respectively, denoting synergistic cooperative adsorption (R_q and $1/n > 1$). In the single solute system, ultrahigh maximum monolayer adsorption capacity of 2803 and 3659 mg g^{-1} was observed for CV and Cr(VI) respectively. Adsorption energies supported the physisorption-mediated pseudo-first-order model a better model to describe the adsorption rates in single and binary systems. This study opens up new questions on the mechanisms involved in the adsorption of pollutants in multicomponent systems.

Author contributions

All authors contributed to the review conception, writing sections of the original manuscript, and reviewing of manuscript. All authors read and approved the final manuscript.

Data availability

The data used to support the findings of this study are included within the article.

Conflicts of interest

The authors have no relevant financial or non-financial interests to disclose.

Acknowledgements

The authors declare that no funds, grants, or other support were received during the preparation of this manuscript.

References

1 J. Davidovits, *GEOPOLYMER CEMENTGeopolymer Cement a review, published in Geopolymer Science and Technics, Technical*, Geopolymer Institute Library, 2013, pp. 1–11, **https://www.geopolymer.org**.

2 S. N. Fifinatasha, A. M. Mustafa Al Bakri, H. Kamarudin, Y. Zarina, A. R. Rafiza and J. Liyana, Reviews on the different sources materials to the geopolymer performance, *Adv. Environ. Biol.*, 2013, 7(12), 3835–3842.

3 P. Cong and Y. Cheng, Advances in geopolymer materials: a comprehensive review, *J. Traffic Transp. Eng.*, 2021, **8**(3), 283–314, DOI: **10.1016/j.jtte.2021.03.004**.

4 I. Luttah, D. O. Onunga and V. O. Shikuku, Removal of endosulfan from water by municipal waste incineration fl y ash-based geopolymers: Adsorption kinetics, isotherms, and thermodynamics, *Environ. Chem.*, 2023, **4**, 1164372.

5 A. M. Elgarahy, A. Maged, M. G. Eloffy, M. Zahran, S. Kharbish and K. Z. Elwakeel, *et al.*, Geopolymers as sustainable eco-friendly materials: classification, synthesis routes, and applications in wastewater treatment, *Sep. Purif. Technol.*, 2023, **324**, 124631, DOI: **10.1016/j.seppur.2023.124631**.

6 S. Mani and R. N. Bharagava, Exposure to crystal violet, its toxic, genotoxic and carcinogenic effects on environment and its degradation and detoxification for environmental safety, *Rev. Environ. Contam. Toxicol.*, 2016, **237**, 71–104.

7 H. Hossini, B. Shafie, A. D. Niri, M. Nazari, A. J. Esfahlan and M. Ahmadpour, *et al.*, A comprehensive review on human health effects of chromium: insights on induced toxicity, *Environ. Sci. Pollut. Res.*, 2022, **29**(47), 70686–70705, DOI: **10.1007/s11356-022-22705-6**.

8 P. Sharma, S. P. Singh, S. K. Parakh and Y. W. Tong, Health hazards of hexavalent chromium (Cr(VI)) and its microbial

reduction, *Bioengineered*, 2022, **13**(3), 4923–4938, DOI: 10.1080/21655979.2022.2037273.

9 J. Qiu, Y. Zhao, J. Xing and X. Sun, Fly ash-based geopolymer as a potential adsorbent for Cr(VI) removal, *Desalin. Water Treat.*, 2017, **70**, 201–209.

10 J. Grillo, A. M. Montao and C. P. Gonzalez, Use of synthetic polymers of pumice for the removal of chromium in the tannery industry, *J. Phys.: Conf. Ser.*, 2020, **1645**(1), 2–8.

11 J. A. López, A. M. Montao, C. P. González and L. Medina, Evaluation of the methyl violet sorption capacity in waters with a bentonite based geopolymer material, *J. Phys.: Conf. Ser.*, 2020, **1587**(1), 7.

12 M. B. Jacques, N. P. Guy, M. L. Jules, Z. P. Harlette, M. E. Judith and M. Said, *et al.*, Removal of crystal violet by – TiO_2 loaded alkali – activated carbon hybrid material from Raphia farinifera fruit kernels: surface chemistry, parameters and mechanisms, *Biomass Convers. Biorefin.*, 2023, **0123456789**, 1–21.

13 A. S. Sidjou, A. N. Tchakounte, V. Shikuku, I. Lenou, R. Djimtibaye and M. M. Dika, Synthesis of alkali-activated volcanic scoria and rice husk ash based composite materials for adsorptive removal of crystal violet: Optimization, kinetics, isotherms and mechanism, *Hybrid Adv.*, 2023, **4**, 100113.

14 C. Sarkar, J. K. Basu and A. N. Samanta, Experimental and kinetic study of fluoride adsorption by Ni and Zn modified LD slag based geopolymer, *Chem. Eng. Res. Des.*, 2018, **142**, 165–175, DOI: 10.1016/j.cherd.2018.12.006.

15 V. O. Shikuku, S. Tome, D. T. Hermann, G. A. Tompsett and M. T. Timko, Rapid Adsorption of Cationic Methylene Blue Dye onto Volcanic Ash – metakaolin Based Geopolymers, *Silicon*, 2022, **14**(15), 9349–9359, DOI: 10.1007/s12633-021-01637-9.

16 S. Tome, V. Shikuku, H. Dzoujo, S. Akiri, M. Annie and C. Rüscher, *et al.*, Efficient sequestration of malachite green in aqueous solution by laterite – rice husk ash – based alkali – activated materials: parameters and mechanism, *Environ. Sci. Pollut. Res.*, 2023, 1–15, DOI: 10.1007/s11356-023-27138-3.

17 J. Zhang, Y. Ge, Z. Li and Y. Wang, Facile fabrication of a low-cost and environmentally friendly inorganic-organic composite membrane for aquatic dye removal, *J. Environ. Manage.*, 2020, **256**, 109969, DOI: 10.1016/j.jenvman.2019.109969.

18 P. Y. He, Y. J. Zhang, H. Chen, Z. C. Han and L. C. Liu, Low-cost and facile synthesis of geopolymer-zeolite composite membrane for chromium(VI) separation from aqueous solution, *J. Hazard. Mater.*, 2020, **392**(13), 122359, DOI: 10.1016/j.jhazmat.2020.122359.

19 Y. Fang, L. Yang, F. Rao, K. Zhang, Z. Qin and Z. Song, *et al.*, Behaviors and Mechanisms of Adsorption of MB and Cr(VI) by Geopolymer Microspheres under Single and Binary Systems, *Molecules*, 2024, (Vi), 1–16.

20 Z. Yu, W. Song, J. Li and Q. Li, Improved simultaneous adsorption of Cu(II) and Cr(VI) of organic modified metakaolin-based geopolymer, *Arabian J. Chem.*, 2020, **13**(3), 4811–4823, DOI: 10.1016/j.arabjc.2020.01.001.

21 H. Dzoujo Tamaguelon, V. O. Shikuku, S. Tome, S. Akiri, N. M. Kengne and S. Abdpour, *et al.*, Synthesis of pozzolan and sugarcane bagasse derived geopolymer-biochar composites for methylene blue sequestration from aqueous medium, *J. Environ. Manage.*, 2022, **318**, 115533, DOI: 10.1016/j.jenvman.2022.115533.

22 H. Dzoujo, V. Odhiambo, S. Tome, F. Gallo, P. Ondiek and T. Strothmann, *et al.*, Unary adsorption of sulfonamide antibiotics onto pozzolan-tyre ash based geopolymers: Isotherms, kinetics and mechanisms, *Chem. Eng. Res. Des.*, 2024, **206**, 440–452, DOI: 10.1016/j.cherd.2024.05.009.

23 J. M. Mboka, H. D. Tamaguelon, V. Shikuku, S. Tome, V. F. Deugueu and H. Othman, *et al.*, Novel Superadsorbent from Pozzolan-Charcoal based Geopolymer Composite for the Efficient Removal of Aqueous Crystal Violet, *Water, Air, Soil Poll.*, 2024, **235**(6), 1–17, DOI: 10.1007/s11270-024-07257-4.

24 T. H. Dzoujo, S. Tome, V. O. Shikuku, J. B. Tchuigwa, A. Spieß and C. Janiak, *et al.*, Enhanced Performance of Hydrogen Peroxide Modified Pozzolan-Based Geopolymer for Abatement of Methylene Blue from Aqueous Medium, *Silicon*, 2021, **14**(10), 5191–5206.

25 E. Jusli, H. Nor, R. P. Jaya and Z. Haron, Chemical Properties of Waste Tyre Rubber Granules, *Adv. Mater. Res.*, 2014, **911**, 77–81.

26 A. Saud, N. Nadiah, M. Firdaus, S. Rangabhashiyam, H. Jawad and L. D. Wilson, *et al.*, Statistical modeling and mechanistic pathway for methylene blue dye removal by high surface area and mesoporous grass-based activated carbon using K_2CO_3 activator, *J. Environ. Chem. Eng.*, 2021, **9**(4), 105530, DOI: 10.1016/j.jece.2021.105530.

27 A. Islam, M. J. Ahmed, W. A. Khanday, M. Asif and B. H. Hameed, Mesoporous activated coconut shell-derived hydrochar prepared via hydrothermal carbonization-NaOH activation for methylene blue adsorption, *J. Environ. Manage.*, 2017, **203**, 237–244, DOI: 10.1016/j.jenvman.2017.07.029.

28 D. Shen, C. Wen, M. O. Adebajo, G. Chen and W. Hua, Applied Clay Science Adsorption of methylene blue from aqueous solution onto porous cellulose-derived carbon/montmorillonite nanocomposites, *Appl. Clay Sci.*, 2018, **161**, 256–264, DOI: 10.1016/j.clay.2018.02.017.

29 S. Tome, M. A. Etoh, J. Etame and S. Kumar, Improved Reactivity of Volcanic Ash using Municipal Solid Incinerator Fly Ash for Alkali-Activated Cement Synthesis, *Waste Biomass Valoriz.*, 2020, **11**(6), 3035–3044.

30 T. R. Barbosa, E. L. Foletto, G. L. Dotto and S. L. Jahn, Preparation of mesoporous geopolymer using metakaolin and rice husk ash as synthesis precursors and its use as potential adsorbent to remove organic dye from aqueous solutions, *Ceram. Int.*, 2018, **44**(1), 416–423.

31 A. Deb, A. Debnath and B. Saha, Sono-assisted enhanced adsorption of eriochrome Black-T dye onto a novel polymeric nanocomposite: kinetic, isotherm, and response surface methodology optimization, *J. Dispersion Sci. Technol.*, 2020, **42**(11), 1579–1592, DOI: 10.1080/01932691.2020.1775093.

32 A. Deb, A. Debnath, N. Bhattacharjee and B. Saha, Ultrasonically enhanced dye removal using conducting polymer functionalised ZnO nanocomposite at near neutral pH: kinetic study, isotherm modelling and adsorbent cost analysis, *Int. J. Environ. Anal. Chem.*, 2020, **102**(19), 8055–8074, DOI: 10.1080/03067319.2020.1843649.
33 D. Yankwa Jean Noel, S. Kumar and H. K. T. Antoine Elimbi, Reactivity of volcanic ash in alkaline medium, microstructural and strength characteristics of resulting geopolymers under different synthesis conditions, *J. Mater. Sci.*, 2016, **51**, 10301–10317.
34 Y. S. Ho and G. Mckay, Sorption of dye from aqueous solution by peat, *Chem. Eng. J.*, 1998, **70**, 115–124.
35 Y. Ho, Review of second-order models for adsorption systems, *J. Hazard. Mater.*, 2006, **136**, 681–689.
36 W. J. Weber, JCM. Kinetics of adsorption on carbon from solutions, *J. Sanit. Eng. Div., Am. Soc. Civ. Eng.*, 1963, **89**(2), 31–39.
37 A. Deb, A. Debnath and B. Saha, Ultrasound-aided rapid and enhanced adsorption of anionic dyes from binary dye matrix onto novel hematite/polyaniline nanocomposite: response surface methodology optimization, *Appl. Organomet. Chem.*, 2019, **34**(2), 1–20.
38 I. Langmuir, The constitution and fundamental properties of solids and liquids. Part II.-Liquids, *J. Franklin Inst.*, 1917, **184**(5), 721.
39 V. O. Shikuku, R. Zanella, C. O. Kowenje, F. F. Donato, N. M. G. Bandeira and O. D. Prestes, Single and binary adsorption of sulfonamide antibiotics onto iron-modified clay: linear and nonlinear isotherms, kinetics, thermodynamics, and mechanistic studies, *Appl. Water Sci.*, 2018, **8**(6), 1–12, DOI: 10.1007/s13201-018-0825-4.
40 H. Freundlich, Über die Adsorption in Lösungen, *Z. Phys. Chem.*, 1906, **57**(4), 385–470.
41 V. O. Shikuku and T. Mishra, Adsorption isotherm modeling for methylene blue removal onto magnetic kaolinite clay: a comparison of two-parameter isotherms, *Appl. Water Sci.*, 2021, **11**(6), 1–9, DOI: 10.1007/s13201-021-01440-2.
42 P. J. Flory, *Principles of Polymer Chemistry*, Cornell University Press, New York, 1953.
43 S. Chen, Y. Huang, X. Han, Z. Wu, C. Lai and J. Wang, *et al.*, Simultaneous and efficient removal of Cr(VI) and methyl orange on LDHs decorated porous carbons, *Chem. Eng. J.*, 2018, **352**(Vi), 306–315, DOI: 10.1016/j.cej.2018.07.012.
44 R. Soltani, A. Marjani and S. Shirazian, A hierarchical LDH/MOF nanocomposite: Single, simultaneous and consecutive adsorption of a reactive dye and Cr(VI), *Dalton Trans.*, 2020, **49**(16), 5323–5335.
45 C. Zhou, C. Han, X. Min and T. Yang, Simultaneous adsorption of As(V) and Cr(VI) by zeolite supporting sulfide nanoscale zero-valent iron: competitive reaction, affinity and removal mechanism, *J. Mol. Liquids*, 2021, **338**, 116619, DOI: 10.1016/j.molliq.2021.116619.
46 F. Dong, L. Yan, X. Zhou, S. Huang, J. Liang and W. Zhang, Simultaneous adsorption of Cr(VI) and phenol by biochar-based iron oxide composites in water: performance, kinetics and mechanism, *J. Hazard. Mater.*, 2021, **416**, 125930, DOI: 10.1016/j.jhazmat.2021.125930.
47 J. Zolgharnein, M. Bagtash and T. Shariatmanesh, Simultaneous removal of binary mixture of Brilliant Green and Crystal Violet using derivative spectrophotometric determination, multivariate optimization and adsorption characterization of dyes on surfactant modified nano-γ-alumina, *Spectrochim. Acta, Part A*, 2015, **137**, 1016–1028, DOI: 10.1016/j.saa.2014.08.115.
48 U. A. Guler, M. Ersan, E. Tuncel and F. Dügenci, Mono and simultaneous removal of crystal violet and safranin dyes from aqueous solutions by HDTMA-modified Spirulina sp, *Process Saf. Environ. Prot.*, 2016, **99**, 194–206.
49 M. Ashrafi, M. Arab Chamjangali, G. Bagherian and N. Goudarzi, Removal of Brilliant Green and Crystal violet from Mono- and Bi-component Aqueous Solutions Using NaOH-modified Walnut Shell, *Anal. Bioanal. Chem. Res.*, 2018, **5**, 95–114.
50 T. Shen, L. Wang, Q. Zhao, S. Guo and M. Gao, Single and simultaneous adsorption of basic dyes by novel organo-vermiculite: a combined experimental and theoretical study, *Colloids Surf., A*, 2020, **601**, 125059, DOI: 10.1016/j.colsurfa.2020.125059.
51 M. Essandoh, R. A. Garcia, V. L. Palochik, M. R. Gayle and C. Liang, Simultaneous adsorption of acidic and basic dyes onto magnetized polypeptidylated-Hb composites, *Sep. Purif. Technol.*, 2021, **255**, 117701, DOI: 10.1016/j.seppur.2020.117701.
52 H. Kandil and H. Ali, Simultaneous Removal of Cationic Crystal Violet and Anionic Reactive Yellow Dyes using eco-friendly Chitosan Functionalized by Talc and Cloisite 30B, *J. Polym. Environ.*, 2023, **31**(4), 1456–1477, DOI: 10.1007/s10924-022-02682-0.